

Nanoscale organic electroluminescence from tunnel junctionsX.-L. Guo,^{1,*} Z.-C. Dong,¹ A. S. Trifonov,¹ K. Miki,¹ Y. Wakayama,¹ D. Fujita,¹ K. Kimura,¹ S. Yokoyama,² and S. Mashiko²¹National Institute for Materials Science, 1-1 Namiki, Tsukuba 305-0044, Japan²Communication Research Laboratory, Kobe, Hyogo 651-2401, Japan

(Received 7 April 2004; revised manuscript received 11 August 2004; published 27 December 2004)

Nanoscale organic electroluminescence was induced by positioning a sharp tungsten tip on the surface of a free-base porphyrin (H₂TBPP) monolayer on the top of PtTBP porphyrin (PtTBPP) multilayers on a Cu(100) substrate in an ultrahigh vacuum scanning tunneling microscope (STM) system. The well-defined molecular fluorescence spectra are perfectly matched with the conventional photoluminescence spectrum from bulk H₂TBPP molecules. The nanoscale PtTBPP multilayers do not fluoresce; rather, they act as spacers to enhance the decoupling of the electronic state of the H₂TBPP monolayer from the Cu surface. The electronic property of molecules and the energy-level alignment of molecules with respect to the Fermi levels of electrodes are probably quite critical for observing STM-induced molecular fluorescence from molecular layers with a similar thickness. The molecule in proximity to the tip apex of a scanning tunneling microscope is locally excited by the hot electron injection mechanism, followed by radiative decay via Franck-Condon transitions.

DOI: 10.1103/PhysRevB.70.233204

PACS number(s): 68.37.Ef, 73.20.-r, 33.80.-b

A scanning tunneling microscope (STM) is capable of more than imaging with atomic resolution and manipulation; the highly localized tunneling current can also be used as a source of hot electrons or holes to locally excite luminescence from metals, semiconductors, polymers, and molecules.¹⁻¹¹ Among them, nanoscale organic electroluminescence is important for the development of molecular light source, high-resolution optical microscopy^{12,13} and quantum information processing.¹⁴ However, there is still no direct evidence of clear molecular fluorescence in the limited reports on STM-induced optical spectra,^{7-11,15-21} which can be justified by comparison to the conventional photoluminescence from neutral organic molecules. The role of molecules has been suggested to act mainly as a spacer to modify plasmon-mediated emissions.⁹ Nevertheless, STM-induced luminescence spectra were previously observed for polymers, though under field emission conditions (~ 100 V) and on a relatively thick thin film (~ 200 nm).⁶ Qiu *et al.*¹⁰ reported the use of an oxide buffer layer for the detection of single-molecule fluorescence, which is attributed to the transitions between two unoccupied orbitals of a molecular anion rather than neutral molecules. The difficulty in observing clear molecular fluorescence on metal substrates is mainly owing to the nonradiative damping of molecular excited states and the resultant quenching of molecular luminescence on metal substrates.^{22,23} Here we demonstrate a way to generate nanoscale organic electroluminescence from tunnel junctions. A nanoscale PtTBP porphyrin (PtTBPP) buffer layer is used as a spacer to enhance the decoupling of the top H₂TBPP monolayer from the Cu(100) substrate. The molecular origin of luminescence is established by the perfect matching of the observed well-defined molecular fluorescence with the conventional photoluminescence data.

The experiments were carried out in an ultrahigh vacuum (UHV) system with facilities for sample heating and cooling, molecule deposition, and characterization by a STM (JEOL JSTM-4500XT). The base pressure of the system is ~ 2

$\times 10^{-10}$ Pa. The STM tips were made from a tungsten (W) wire by electrochemical etching in a 2N NaOH solution followed by baking and Ar⁺ ion sputtering in UHV. An atomically clean Cu(100) ($3 \times 7 \times 0.5$ mm³) substrate was prepared by several cycles of sputtering (Ar⁺, 1 keV, ~ 1 μ A, 30 min) and annealing (~ 500 °C, 30 min). H₂TBPP and PtTBPP molecules shown in Figs. 1(a) and 1(b) were deposited on Cu(100) in sequence by sublimation from quartz cells at ~ 300 °C. The deposition rate was controlled by a thickness monitor. Compared with other organic molecules, a porphyrin-based molecule possesses two unique properties: (1) It has strong interaction with photons including absorption and fluorescence.²⁴ (2) Each porphyrin molecule (see Fig. 1) has four bulky di-tert-butylphenyl (TBP) groups as legs. The phenyl rings in the four TBP groups are roughly perpendicular to the porphyrin core plane due to the steric repulsion between phenyl and pyrrole H atoms.^{11,25} The porphyrin core is shored up ~ 0.7 nm above the substrate. Thus the porphyrin core plane is decoupled from the metal substrate to some extent. This kind of electronic decoupling is believed to be helpful for reducing the nonradiative energy dissipation to the metal substrate.

Our light collection and detection system have been described elsewhere.²¹ Briefly, photons emitted from the tunneling gap are collected by a lens near the tip-sample gap region and detected by either a photomultiplier (300–800 nm, dark current < 3 counts/ps at -30 °C) or a spectrophotometer (350–850 nm) at a spectral resolution of 9 nm.

Figure 2 shows the typical STM image of PtTBPP molecules adsorbed on a Cu(100) substrate with submonolayer coverage. The STM images of porphyrin-based molecules adsorbed on a Cu(100) substrate exhibit similar characteristic. Each PtTBPP molecule consists of four separated bright lobes with a spacing of ~ 1.9 nm across, which correspond to the four TBP groups in Fig. 1. This indicates that the porphyrin core is oriented parallel to the Cu surface (~ 0.7 nm

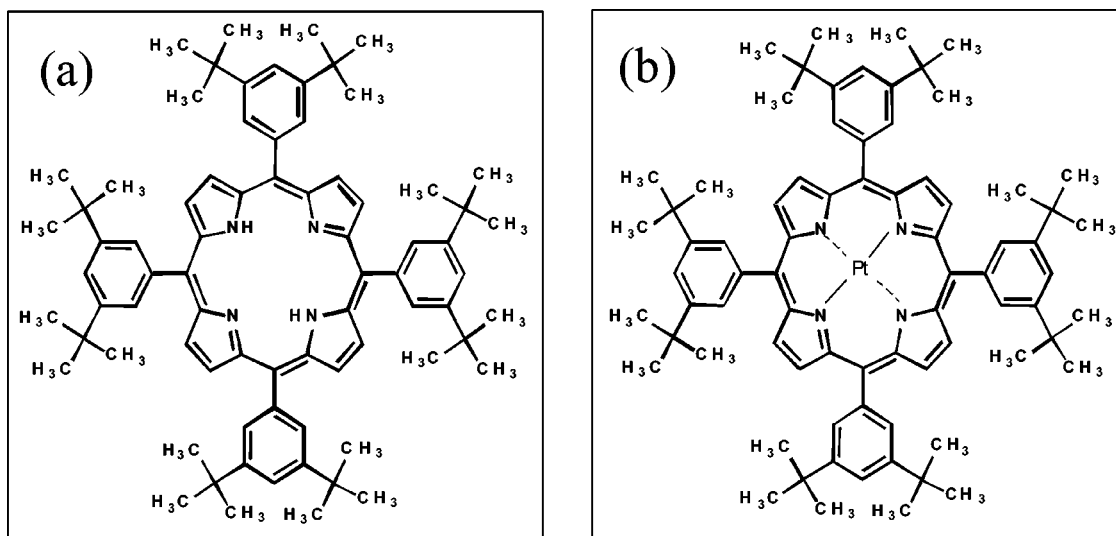


FIG. 1. Molecular structures of H₂TBPP and PtTBPP molecules.

above the Cu surface) and the phenyl rings are tilted.²⁵

Optical spectra are measured by positioning a sharp W tip on the surface of pristine Cu(100), PtTBPP/Cu(100), and H₂TBPP/PtTBPP/Cu(100), respectively. The PtTBPP molecules were deposited on the Cu(100) substrate layer by layer with homogeneous coverage in a nanoscale thickness regime [~ 6 monolayers (ML)]. The H₂TBPP monolayer was deposited on top of nanoscale PtTBPP multilayers. The total thickness of the molecular layer for the sample of H₂TBPP/PtTBPP/Cu(100) is estimated to be less than 5 nm based on the molecular height of ~ 0.7 nm. The imaging resolution of the nanoscale multilayers degrades with increased thickness as a result of unstable tunneling conditions. For comparison, the conventional photoluminescence spectra from bulk H₂TBPP and PtTBPP molecules were also measured by a He—Cd laser at 325 nm. The typical optical spectra were shown in Fig. 3.

The spectrum from PtTBPP multilayers (in the nanoscale thickness regime) on Cu(100) (curve 2) shows a single-peak feature that is the same as that of plasmon-mediated emission from pristine Cu(100) (curve 1). The whole shape of the optical spectrum of curve 2 is similar to that of curve 1 except for the blueshift (~ 9 nm to the peak position of plasmon-mediated emission at 610 nm) and intensity enhancement.^{9,16} The emission peak at 650 nm in curve 4 is absent in curve 2. The nanoscale PtTBPP multilayers on Cu(100) do not fluoresce or their fluorescence is completely quenched on Cu(100). The same feature was found for the H₂TBPP monolayer on Cu(100). Thus, further electronic decoupling is required to weaken the molecule-substrate interaction for generating molecular fluorescence.

Since energy transfer near a surface depends dramatically on the fluorophore-substrate distance,²² we deposit one H₂TBPP monolayer directly on the top of the nanoscale PtTBPP multilayers on Cu(100). The bottom nanoscale PtTBPP multilayers are used as a spacer layer to increase the fluorophore-substrate distance.

Curve 3 shows the typical spectra from the surface of nanoscale H₂TBPP/PtTBPP/Cu(100) multilayers. New

peaks at 658 and 723 nm appeared, i.e., these two well-defined peaks are absent for pristine Cu(100) and nanoscale PtTBPP/Cu(100) multilayers. The molecular origin of these peaks is evident and is further justified by comparison with the peak positions in the standard photoluminescence spectra (curve 5). These two peak positions in curves 3 and 5 match perfectly.

It is worth noting that a weak plasmon-mediated emission band from the Cu substrate at ~ 610 nm is still discernable in curve 3, but with a much lower intensity with respect to that from the pristine Cu(100) surface under approximately the same tunneling condition as that for curves 1 and 2. Since the plasmon-mediated emissions originate from inelastic tun-

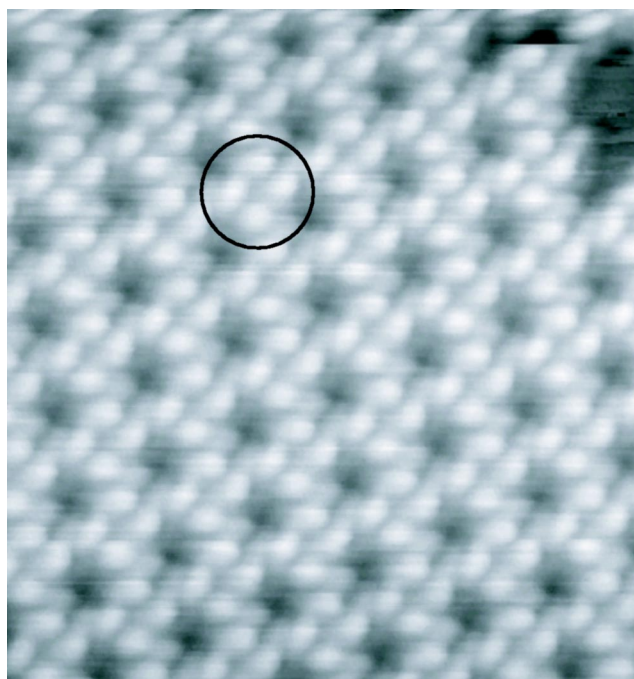


FIG. 2. STM image of PtTBPP submonolayer on Cu(100) (16×16 nm², 2.0 V, 0.1 nA).

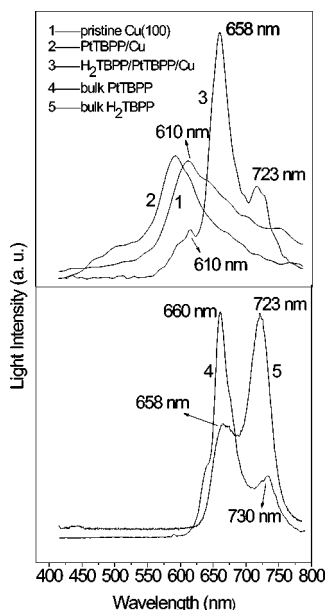


FIG. 3. STM-induced light emission spectra from the surface of pristine Cu(100) (curve 1: 2.5 V, 1.5 nA), PtTBPP/Cu(100) (curve 2: 2.5 V, 1.5 nA, H₂TBPP/PtTBPP/Cu(100) (curve 3: 2.8 V, 1.5 nA), and the photoluminescence spectra from bulk PtTBPP (curve 4) and H₂TBPP molecules (curve 5) excited by a He-Cd laser at 325 nm.

neling excitations of interface plasmon modes between the tip and the Cu substrate, the thickness increase of the molecular layer weakens both the local electromagnetic field strength across the junction and the molecule-substrate interaction, leading to a decreased intensity.

An interesting phenomenon is that the observed molecular fluorescence exists at both polarities as typically shown in Fig. 4, which presents a unique demonstration of “bipolar” nanoscale organic electroluminescence and also a promise of AC operation. The higher intensity at positive bias indicates higher electron injection efficiency from the tungsten tip than from the Cu substrate due to the high electric field in proximity the tip apex. The H₂TBPP molecule is a hole transport material typical of aromatic compounds.²⁶ The majority hole carriers are readily available in the molecular layer through hopping by thermal or multi-vibrational excitation.²⁶ Consequently, the decisive factor for generating molecular fluorescence from H₂TBPP is the injection efficiency of minority electron carriers from the metal tip or substrate. Once electrons are injected into the LUMO, they can subsequently recombine with the holes in the HOMO to emit light. The inset of Fig. 4 plots the observed emission intensity versus the tunnel current at a fixed voltage of +2.8 V. The current dependency of emission intensity follows nearly a linear relation.

It is worth pointing out that molecular fluorescence has been generated from the surface of H₂TBPP multilayers on Au(100) and ZnTBPP multilayers on Cu(100) in a similar nanoscale thickness regime available for electron tunneling^{27,28} with that of PtTBPP multilayers on Cu(100). Other widely used luminescent molecules such as Alq3 (to be reported in a future paper) are the same as PtTBPP, which

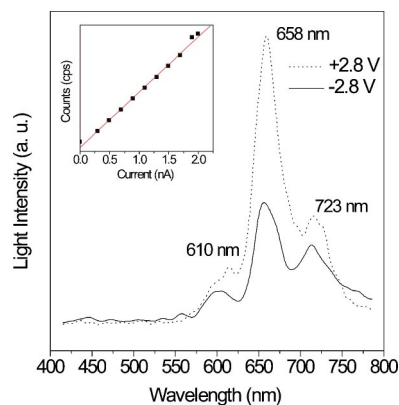


FIG. 4. STM-induced molecular fluorescence from the surface of H₂TBPP/PtTBPP/Cu(100) at both polarities (tunneling current = 1.5 nA). The inset shows the linear dependence of photon emission intensity vs tunnel current.

does not fluoresce even under the same thickness regime, and with the STM excitation condition as the aforementioned molecular multilayers. This indicates that under the similar film thickness, the STM-induced molecular luminescence is sensitive to the chemical compounds as well as the film quality. The electronic property of molecules and the energy-level alignment of molecules with respect to the Fermi levels of electrodes are probably quite critical for observing STM-induced molecular fluorescence. Molecules act as a functional unit, not just as a resistor in the observed STM-induced molecular fluorescence. Both HOMO and LUMO orbitals have to be involved in the luminescence process. We have not explored much the effect of film quality on STM-induced molecular luminescence, but an ordered film or a disordered film should cause some differences in the molecular fluorescence process. A certain degree of energy disorder appears also to be important for carriers to hop around.

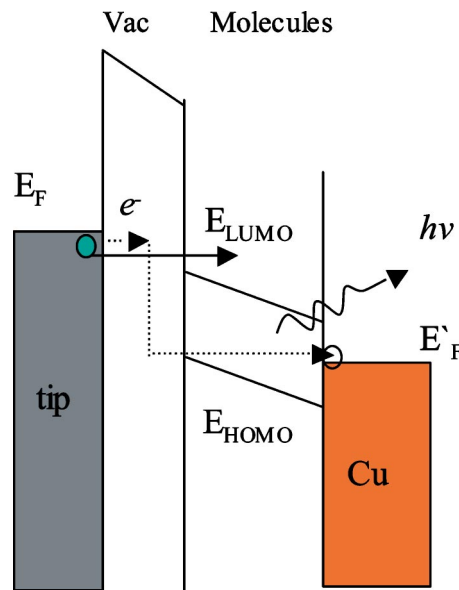


FIG. 5. A schematic energy diagram showing two possible processes for luminescence excitation, i.e., inelastic electron tunneling (dashed arrow line) and hot electron injection (solid arrow line).

The emission mechanism of STM-induced molecular fluorescence can be explained by Fig. 5. There are probably two processes participating in the emission, i.e., inelastic electron tunneling (IET) and hot electron injection (HEI), which is schematically shown by the dashed arrow line and solid arrow line, respectively, in Fig. 5.

In the IET process, the plasmon-mediated emission is generated via direct tunneling excitation from the tip to the substrate, or electron tunneling into unoccupied molecular orbitals, followed by the nonradiative energy transfer from excited molecular anionic states to the surface plasmons. In the hot electron injection process, electrons tunnel elastically across the vacuum gap and into the unoccupied orbitals of the H₂TBPP molecules followed by radiative decay. Based on the experimental results in Fig. 4, molecular fluorescence is probably generated when the charged molecules decay radiatively via Frank-Condon transitions.

In summary, nanoscale molecular luminescence from tunnel junctions has been observed by depositing the H₂TBPP monolayer on top of nanoscale PtTBPP multilayers on Cu(100). The generated molecular fluorescence is well defined and is perfectly matched with the conventional photolumi-

nescence data from bulk H₂TBPP molecules. No molecular luminescence was observed from PtTBPP multilayers on Cu(100) in the nanoscale thickness regime. The nanoscale PtTBPP multilayers act as a spacer to enhance the decoupling of the electronic state of the top H₂TBPP monolayer from the Cu(100) substrate. Under a similar film thickness of molecules, the STM-induced molecular luminescence is sensitive to the electronic property of molecules and the energy-level alignment of molecules with respect to the Fermi levels of electrodes, and the film quality. Molecules act as a functional unit, not just as a resistor in the observed STM-induced molecular fluorescence. The molecular emission mechanism is probably attributed to the hot electron injection to the molecules in proximity to the tip apex of a scanning tunneling microscope, followed by a radiative decay via Frank-Condon transitions. This research opens alternative routes to the development of nanoscale organic light source and spectroscopy.

This study was performed through Special Coordination Funds of the Ministry of Education, Culture, Sports, Science and Technology (MEXT) of the Japanese Government.

*Corresponding author: Fax: +81-29-859-2801. Email address: Guo.Xinli@nims.go.jp

¹J. H. Coombs, J. K. Gimzewski, B. Reihl, J. K. Sass, and R. R. Schlittler, *J. Microsc.* **152**, 325 (1988).

²R. Berndt, J. K. Gimzewski, and P. Johansson, *Phys. Rev. Lett.* **67**, 3796 (1991).

³D. L. Abraham, A. Veider, C. Schonenberger, H. P. Meier, D. J. Arent, and S. F. Alvarado, *Appl. Phys. Lett.* **56**, 1564 (1990).

⁴Y. Uehara, T. Fujita, and S. Ushioda, *Phys. Rev. Lett.* **83**, 2445 (1999).

⁵C. Thirstrup, M. Sakurai, K. Stokbro, and M. Aono, *Phys. Rev. Lett.* **82**, 1241 (1978).

⁶S. F. Alvarado, W. Rieß, P. F. Seidler, and P. Strohhriegl, *Phys. Rev. B* **56**, 1269 (1997).

⁷S. F. Alvarado, L. Libioulle, and P. F. Seidler, *Synth. Met.* **91**, 69 (1997).

⁸R. Berndt, R. Gaisch, J. K. Gimzewski, B. Reihl, R. R. Schlittler, W. D. Schneider, and M. Tschudy, *Science* **262**, 1425 (1993).

⁹G. Hoffmann, L. Libioulle, and R. Berndt, *Phys. Rev. B* **65**, 212107 (2002).

¹⁰X. H. Qiu, G. V. Nazin, and W. Ho, *Science* **299**, 542 (2003).

¹¹Z.-C. Dong, A. S. Trifonov, X.-L. Guo, K. Amemiya, S. Yokoyama, T. Kamikado, T. Yamada, S. Mashiko, and T. Okamoto, *Surf. Sci.* **532-535**, 237 (2003).

¹²R. Kopelman and W. Tan, *Science* **262**, 1382 (1993).

¹³J. Michaelis, C. Hettich, J. Mlynek, and V. Sandoghdar, *Nature (London)* **405**, 325 (2000).

¹⁴B. Lounis and W. E. Moerner, *Science* **407**, 491 (2000).

¹⁵Z.-C. Dong, A. Kar, P. Dorozhkin, K. Amemiya, T. Uchihashi, S. Yokoyama, T. Kamikado, S. Mashiko, and T. Okamoto, *Thin*

Solid Films **438-439**, 262 (2003).

¹⁶X.-L. Guo, Z.-C. Dong, A. S. Trifonov, S. Mashiko, and T. Okamoto, *Phys. Rev. B* **68**, 113403 (2003).

¹⁷Z.-C. Dong, A. Tar, Z. Q. Zhou, T. Ohgi, P. Dorozhkin, D. Fujita, S. Yokoyama, T. Terui, T. Yamada, T. Kamikado, M. N. Zhou, S. Mashiko, and T. Okamoto, *Jpn. J. Appl. Phys., Part 1* **41**, 4898 (2002).

¹⁸K. Sakamoto, K. Meguro, R. Arafune, M. Satoh, Y. Uehara, and S. Ushioda, *Surf. Sci.* **502-503**, 149 (2002).

¹⁹G. E. Poirier, *Phys. Rev. Lett.* **86**, 83 (2001).

²⁰F. Touhari, E. J. A. Stoffels, J. W. Gerritsen, H. V. Kempen, and P. Callant, *Appl. Phys. Lett.* **79**, 527 (2001).

²¹X.-L. Guo, Z.-C. Dong, A. S. Trifonov, S. Mashiko, and T. Okamoto, *Jpn. J. Appl. Phys., Part 1* **42**, 6937 (2003).

²²R. R. Chance, A. Prock, and R. Silbey, *Adv. Chem. Phys.* **37**, 1 (1978).

²³W. L. Barnes, *J. Mod. Opt.* **45**, 661 (1998).

²⁴D. Fujita, T. Ohgi, W.-L. Deng, K. Ishige, T. Okamoto, S. Yokoyama, T. Kamikado, and S. Mashiko, *Surf. Sci.* **454-456**, 1021 (2000).

²⁵T. A. Jung, R. R. Schlittler, and J. K. Gimzewski, *Nature (London)* **386**, 696 (1997).

²⁶M. Stolka, J. F. Yanus, and D. M. Pai, *J. Phys. Chem.* **88**, 4707 (1984).

²⁷Z.-C. Dong, X.-L. Guo, A. S. Trifonov, P. Dorozhkin, K. Miki, K. Kimura, S. Yokoyama, S. Mashiko, *Phys. Rev. Lett.* **92**, 086801 (2004).

²⁸X.-L. Guo, Z.-C. Dong, A. S. Trifonov, K. Miki, Y. Wakayama, K. Kimura, S. Yokoyama, and S. Mashiko, *Nanotechnology* **15**, S402 (2004).